Applied Catalysis B: Environmental 187 (2016) 301–309

Contents lists available at ScienceDirect

Applied Catalysis B: Environmental

journal homepage: www.elsevier.com/locate/apcatb

Highly efficient $Bi_2O_2CO_3$/BiOCl photocatalyst based on heterojunction with enhanced dye-sensitization under visible light

Linhui Yu, Xiaoyun Zhang, Guowei Li, Yuantao Cao, Yu Shao, Danzhen Li*

Research Institute of Photocatalysis, State Key Laboratory of Photocatalysis on Energy and Environment, Fuzhou University, Fuzhou 350002, PR China

ARTICLE INFO

Article history:
Received 5 December 2015
Received in revised form 10 January 2016
Accepted 19 January 2016
Available online 22 January 2016

Keywords:
$Bi_2O_2CO_3$/BiOCl
Photocatalyst
Heterostructure
Dye-sensitization
Visible light

ABSTRACT

A facile approach is developed to synthesis the highly efficient photocatalyst of $Bi_2O_2CO_3$/BiOCl. The composite of $Bi_2O_2CO_3$/BiOCl exhibits excellent photocatalytic activity toward Rhodamine B (RhB) under visible light, which is even better than that of P25 (commercial TiO_2) under UV light. The role of the active species in the process of the degradation is evaluated by using different types of active species scavengers and measurement of electron spin resonance (ESR). The relative band structures of the $Bi_2O_2CO_3$ and BiOCl are determined combined with the flat potential (V_{fb}) and bandgap energy (Eg) evaluated by UV–vis diffuse reflectance spectra. The results show that the composite of the two semiconductors facilitates the photosensitized degradation of RhB under visible light ($420\,nm < \lambda < 800\,nm$). And the essence of RhB photosensitization is revealed to be the increase of H_2O_2 in the reaction system. The photocatalytic mechanism is further proposed, which unfolds the charge transfer and the active species formed in the photcatalytic process. The work may set foundation for application of the new photocatalyst of $Bi_2O_2CO_3$-based heterostructure.

1. Introduction

Photocatalysis as a potential technology in application of remedying environmental pollution has become one of the immediate areas of research focus in the last few decades. And the pursuit of a better photocatalyst is never, ever stopped. Photocatalysts responding to the visible light are urgent demand in the photocatalysis science because of the broadening of the response to the sunlight, and in other words the amelioration will improve the utilization of the sunlight. Bismuth-containing compounds have caught much attention these years, and most of them can be excited by visible light. Bi_2O_3 [1,2] and Bi_2S_3 [3,4] as visible-light responsible photocatalysts are well developed and coupled with TiO_2. Bi-based oxysalt photocatalysts, such as $BiVO_4$ [5,6], Bi_2WO_6 [7,8], Bi_2MoO_6 [9,10], $BiPO_4$ [11,12], $Bi_2O_2CO_3$ [13,14] and BiOX (X = Cl, Br, I) [15,16] have showed excellent photocatalytic properties under visible light as reported in the past years.

$Bi_2O_2CO_3$ as a widely used material has long been applied in medical and healthcare purposes. These years, its application in photocatalysis has been explored, and it is ascribed to the aurivillius structure [14], which is layered with alternative stacking $(Bi_2O_2)^{2+}$ sheets interleaved by CO_3^{2-} groups [17]. It is reported that $Bi_2O_2CO_3$ and its coupled composites present good photocatalytic properties [14,18–25]. BiOX (X = Cl, Br, I) as another species of bismuth-based materials have become the hotspot in photocatalysis. The unique properties of high dipole, indirect band gaps, high redox potential of the holes, low recombination rates of electron-hole, and the easily formed oxygen vacancies make BiOX a series of candidate photocatalysts. And the literatures reported corroborate the alternative role of BiOX in the application of photocatalysis [26]. Moreover, the two dimensional BiOX shows layered structure, which is conducive to the transfer and separation of the photo-induced electron and hole [27,28], and the similar layered structures may easily help to form the heterostructure with $Bi_2O_2CO_3$ as well.

There are a few reports on the heterostructure of $Bi_2O_2CO_3$/BiOCl [29–31], and the systematic study on this heterostructure material is lacking. Furthermore, the contrastive photocatalytic property of the $Bi_2O_2CO_3$/BiOCl to other photocatalyst is absent. What is noteworthy in this paper, the photocatalytic activity of $Bi_2O_2CO_3$/BiOCl under visible light is even better than that of P25 under UV light toward the degradation of Rhodamine B (RhB). The heterostructure may be responsible for the excellent photocatalytic property of the material, which utilizes the efficiently photosensitization of RhB over BiOCl [32–34], as well the visible-light responding of the $Bi_2O_2CO_3$. The increase of H_2O_2 in the reaction system is revealed to be closely related to the photosensitization of RhB. And with the assistance of

* Corresponding author.
E-mail addresses: dzli@fzu.edu.cn, danzli@126.com (D. Li).

http://dx.doi.org/10.1016/j.apcatb.2016.01.045
0926-3373/

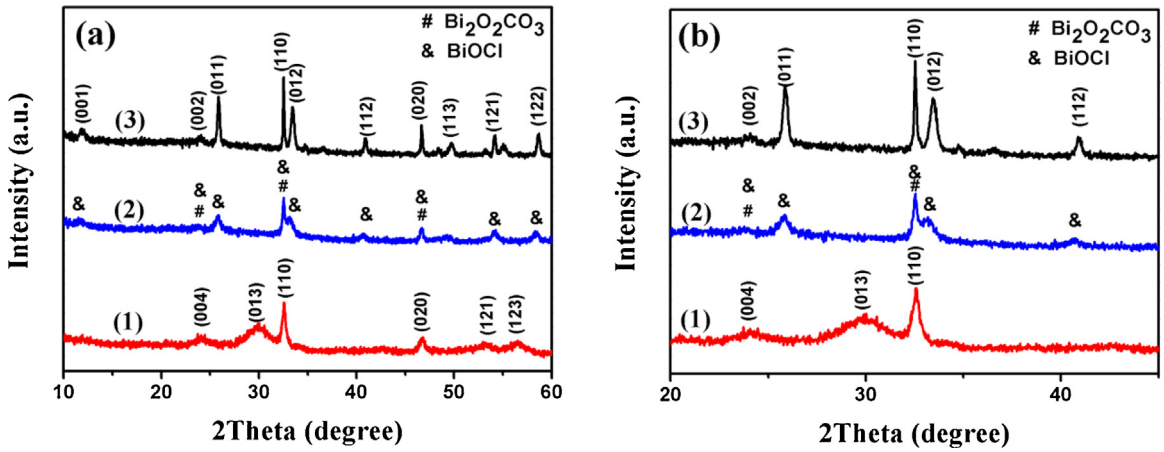

Fig. 1. XRD patterns of (a) and the enlarged view (b) of (1) pure $Bi_2O_2CO_3$, (2) $Bi_2O_2CO_3$/BiOCl composite, (3) pure BiOCl.

dye photosensitization, the excellent photocatalytic property of $Bi_2O_2CO_3$/BiOCl exhibits.

The heterostructure between $Bi_2O_2CO_3$ and BiOCl was prepared via in-situ growth of BiOCl in precursor of $Bi_2O_2CO_3$. The excellent photocatalytic property of the $Bi_2O_2CO_3$/BiOCl is determined by the photocatalytic degradation of RhB under the visible light. The heterostructure between $Bi_2O_2CO_3$ and BiOCl is responsible for the excellent photocatalytic activity, which promotes the charge transfer in the reaction process that makes the hole (h^+) dominate role in the degradation process. Moreover the heterostructure between $Bi_2O_2CO_3$ and BiOCl facilitating the dye-sensitization, which is demonstrated of increasing the H_2O_2 in the reaction system, also makes contribution to the photocatalytic degradation of dye. The role of the active species in the process of the degradation is evaluated by using different types of active species scavengers. And the photocatalytic mechanism is proposed. The work may set foundation for application of the new photocatalyst of $Bi_2O_2CO_3$-based heterostructure.

2. Experimental

2.1. Materials

Bismuth nitrate pentahydrate ($Bi(NO_3)_3{\cdot}5H_2O$), bismuth chloride ($BiCl_3$), carbamide (CH_4N_2O), hydrochloric acid (HCl), cetyltrimethylammonium bromide (CTAB), and ethanol are purchased from Sinopharm Chemical Reagent Co., Ltd., Shanghai, China. All the reagents are analytical grade and used without further purification.

2.2. Systhesis of $Bi_2O_2CO_3$/BiOCl

2.2.1. Preparation of $Bi_2O_2CO_3$

The precursor of $Bi_2O_2CO_3$ was prepared via hydrothermal method. First of all, 2.45 g $Bi(NO_3)_3{\cdot}5H_2O$ was dissolved in 70 mL ethanol. After the absolutely formation of the solution, 0.5 g CH_4N_2O and 0.5 g cetyltrimethylammonium bromide (CTAB) were added with subsequent stirring at room temperature. Then the mixture in the teflon liner was sealed in a stainless steel autoclave and maintained at 180 °C for 12 h. After cooled naturally to ambient temperature, the resultant products were washed several times with water/ethanol and then dried in vacuum at 60 °C. The BiOCl was prepared in the similar method using 0.005 mol $BiCl_3$ instead of $Bi(NO_3)_3{\cdot}5H_2O$.

2.2.2. Preparation of $Bi_2O_2CO_3$/BiOCl

The as prepared $Bi_2O_2CO_3$ sample was further used for the synthesis of $Bi_2O_2CO_3$/BiOCl. The suspension of 0.5 g as-prepared $Bi_2O_2CO_3$ dissolved in 40 mL deionized water was dispersed by ultrasonic treating. Then 3 mL HCl solution, with HCl volume fraction of 5%, was dropwise added to the suspension with stirring for 2 h. And after that, the precipitation was washed with deionized water. Subsequently, the product was dried in vacuum at 60 °C.

2.3. Characterization

The phase constituents of the products were determined by X-ray powder diffractometer (XRD, Bruker D8 Advance with Ni-filtered Cu Kα radiation, λα = 0.15406 nm) at 40 kV and 40 mA in the 2θ range from 10° to 60° with a scan rate of 0.02° per second. The optical properties of the samples were analyzed by UV–vis diffuse reflectance spectroscopy (UV–vis DRS) using a UV–vis spectrophotometer (Cary-500, Varian Co.), in which $BaSO_4$ was used as the background. The morphologies of the obtained products were observed by field-emission scanning electron microscopy (FE-SEM, FEI Nova NANOSEM 230, operated at an accelerating voltage of 15 kV) as well as a transmission electron microscopy (TEM) (FEI Tecnai G2 F20 S-TWIN, operated at an accelerating voltage of 200 kV). X-ray photoelectron spectroscopy (XPS) measurement was performed on a Thermo Scientific ESCA Lab250 spectrometer which consists of a monochromatic Al Kα as the X-ray source, a hemispherical analyzer and sample stage with multi-axial adjustability to obtain the surface composition of the sample. All of the binding energies were calibrated by the C1s peak at 284.6 eV. Electron spin resonance (ESR) signal of the radicals spin-trapped by 5,5-dimethyl-l-pyrroline-*N*-oxide (DMPO) was determined on a Bruker EPR A300 spectrometer. Mott-Schottky method was applied to measure the flat potential (V_{fb}) of semiconductor particle films immersed in 0.1 mol/L Na_2SO_4 solution (pH 7), which is carried out in conventional three electrode cells using a CHI660D electrochemical workstation (shanghai Chenhua Instrument Co., Ltd., Shanghai, China).

2.4. Evaluation of photocatalytic properties

The photocatalytic degradations of RhB aqueous solution (2×10^{-5} mol/L) were conducted in a 100 mL pyrex glass vessel with a plane side at ambient temperature controlled by an air-cooling system. The 500 W Xe-arc lamp (Institute of Electric Light, Bejing) was used as the light source. The 420 nm and 800 nm cutoff filters were placed in front of the vessel to ensure that the reactor was irradiated only by visible light ranging from 420 nm to 800 nm.

A photocatalyst (40 mg) was dispersed in 80 mL of RhB solution and stirred for 2 h to ensure the establishment of adsorption-desorption equilibrium. An aliquot (3 mL) was taken at a certain time interval during the experiment and centrifuged (TDL-5-A) to remove the powders. The filtrates were analyzed on a Varian UV–vis spectrophotometer (Cary 50, Varian Co.). The percentage of degradation is reported as C/C_0, which C represents the absorption of pollutants at each irradiated time interval of the main peak of the absorption spectrum, and C_0 represents that of the initial concentration when adsorption-desorption equilibrium was achieved. In the photocatalytic stability experiments, the catalysts were recollected by centrifugation and then re-dispersed in the same RhB aqueous solution for next cycle. Other experimental parameters were same as the first testing.

3. Results and discussion

3.1. Morphology and optical properties of the samples

The phase and crystallographic structure of the products were determined by XRD. Fig. 1(a)–(b) shows the XRD patterns of the as-prepared $Bi_2O_2CO_3$, BiOCl and $Bi_2O_2CO_3$/BiOCl. The diffraction peaks of XRD patterns belong to the standard values of $Bi_2O_2CO_3$ (JCPDS card No. 41-1488) and BiOCl (JCPDS card No. 73-2060), respectively. As clearly shown in Fig. 1(b) in the enlarged view, when BiOCl forms in the composite, the peak at 2θ value of 30.2 that belongs to (0 1 3) face of $Bi_2O_2CO_3$ fades away, and the peak at 2θ value of 33.6 what belongs to (0 1 2) face of BiOCl arises meanwhile. Compared with pure BiOCl, only a weak peak shift of BiOCl/$Bi_2O_2CO_3$ at 33.6° may be ascribed to an unavoidable lattice distortion that has been reported in the BiOCl/$Bi_2O_2CO_3$ system, which may also implies the interaction between $Bi_2O_2CO_3$ and BiOCl [29]. The main characteristic peaks of $Bi_2O_2CO_3$/BiOCl contain the diffraction peaks of $Bi_2O_2CO_3$ and BiOCl, which are signed with distinguishing marks (# is signed for $Bi_2O_2CO_3$ and & for BiOCl). No other crystal phases can be detected in the patterns, suggesting that no impurity species were formed except $Bi_2O_2CO_3$ and BiOCl.

The SEM images show the morphologies of the samples (Fig. 2). As seen from $Bi_2O_2CO_3$, it appears porous morphology. While for BiOCl, flower-like spheres formed regularly by so many nanosheets. In the preparation process, the BiOCl nanosheets take shape vertically in situ of the porous fluffy $Bi_2O_2CO_3$ structure. The coexistence of the $Bi_2O_2CO_3$ and BiOCl break the porous fluffy morphology, and form randomly growth of BiOCl sheets instead, which make the less surface area of $Bi_2O_2CO_3$/BiOCl than that of $Bi_2O_2CO_3$ (seen the BET data in Fig. S1). The in-situ growth should establish intimate contact between $Bi_2O_2CO_3$ and BiOCl that facilitates the carries transfer.

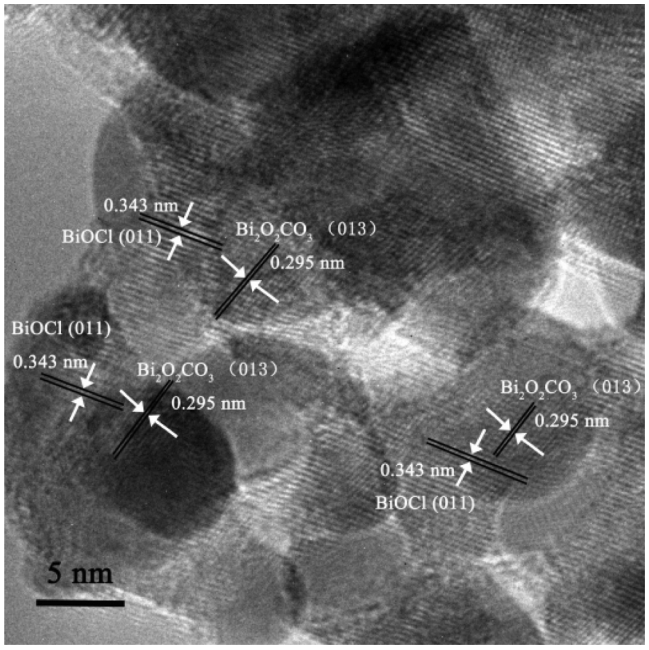

Fig. 3. High-resolution TEM image of the $Bi_2O_2CO_3$/BiOCl composite.

The fine-interconnected particulate morphology and the nanocrystalline nature of the as-prepared $Bi_2O_2CO_3$/BiOCl can be characterized by high-resolution transmission electron microscopy (HRTEM). As can be seen in Fig. 3, the fringes appearing in the micrograph allow the identification of the crystallographic spacing of $Bi_2O_2CO_3$ and BiOCl. The fringe of d = 0.343 nm matches the (0 1 1) crystallographic plane of BiOCl, while the fringe of d = 0.294 nm matches the (0 1 3) crystallographic plane of $Bi_2O_2CO_3$. The particle diameter, as determined from the HRTEM image shown in Fig. 3, is found to be approximately 5 nm for both two components.

To further investigate the surface compositions and chemical state of the as-prepared $Bi_2O_2CO_3$/BiOCl, XPS was carried out, and the results of binding energy spectra are shown in Fig. 4. Fig. 4(a) is the C 1s spectrum, the core lines of which are fixed at 284.6 eV and 288.6 eV. The peak located at 284.6 eV comes from the carbon tape, on which the sample is coated to attach to the sample holder [35], while the peak of 288.6 eV can be ascribed to carbonate ion [36]. The Bi 4f spectrum and the corresponding fitting peaks are

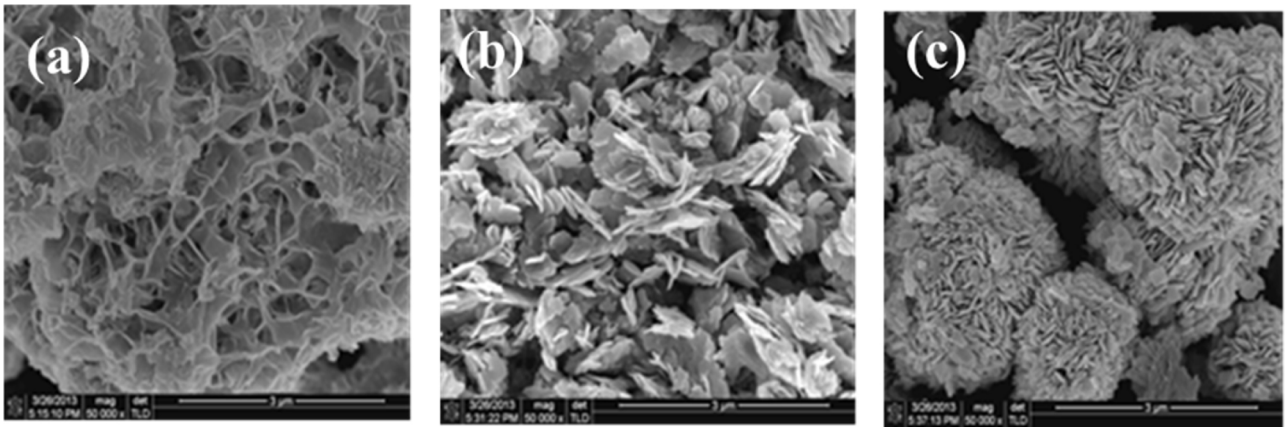

Fig. 2. The SEM images of samples: (a) $Bi_2O_2CO_3$, (b) $Bi_2O_2CO_3$/BiOCl, (c) BiOCl.

shown in Fig. 4(b). The core lines fixed at 158.9 eV and 164.2 eV are indexed to Bi 4f7/2 and Bi 4f5/2, respectively. The O 1s spectrum is shown in Fig. 4(c), which can be fitted by three peaks at binding energies of 530.3, 531.4 and 532.3 eV, respectively. The peak at 530.3 eV is characteristic of Bi-O binding energy, and other two peaks at around 531.4 and 532.3 eV can be assigned to carbonate species and adsorbed H_2O (or surface hydroxyl groups) on the surface [36]. The Cl 2p shown in Fig. 4(d) is resolved into two peaks (197.8, 199.3 eV), which are assigned, respectively, to the Cl 2p3/2 and Cl 2p1/2 regions for BiOCl.

The Fig. 5 represents the UV–vis DRS of as-obtained $Bi_2O_2CO_3$, BiOCl and $Bi_2O_2CO_3$/BiOCl. As can be clearly seen, the optical absorption property of $Bi_2O_2CO_3$/BiOCl is remarkably different from the pure $Bi_2O_2CO_3$ and BiOCl. Comparing with the pure BiOCl, the $Bi_2O_2CO_3$/BiOCl shows a red shift, while with pure $Bi_2O_2CO_3$, a blue shift occurs. Moreover, the $Bi_2O_2CO_3$/BiOCl has a higher absorption in the ultraviolet region than that of $Bi_2O_2CO_3$ and BiOCl. Otherwise, the absorption of visible light (420–800 nm) makes the $Bi_2O_2CO_3$/BiOCl a higher utilization of light. It is well known for crystalline semiconductor that the optical absorption near the band edge follows the equation as follow, [37].

$$F(R)E = A(E - Eg)^{n/2} \quad (1)$$

where F(R), E, A, n, and Eg are diffuse absorption coefficient, photon energy, proportionality constant, an integer (n = 1,2,4,6), and bandgap, respectively. For the material of $Bi_2O_2CO_3$ [17] and BiOCl [28], the value of n is 4. As shown in Fig. 5(b), the estimated Eg is 2.84 eV for $Bi_2O_2CO_3$ and 3.42 eV for BiOCl.

3.2. Photocatalytic properties of the samples

The photocatalytic activity of degradation of RhB (2.0×10^{-5} mol/L) over $Bi_2O_2CO_3$/BiOCl, pure $Bi_2O_2CO_3$ and BiOCl were evaluated under visible light (420 nm < λ < 800 nm) irradiation (shown in Fig. 6). The adsorption-desorption equilibrium of the mixture suspension is established after 2 h of stirring in dark. It clearly shows that RhB solution is hardly degraded without any catalyst under visible light irradiation. With the illumination time increasing, the absorption peak of RhB at 554 nm decreases gradually (Fig. 6(a)). The $Bi_2O_2CO_3$/BiOCl exhibits the best performance and about 98.0% of RhB was degraded over it within 12 min, while $Bi_2O_2CO_3$ and BiOCl take 30 min and 50 min to reach the approximate degradation rate. It is obvious that the photocatalytic activity of $Bi_2O_2CO_3$/BiOCl under visible light is much better than that of pure $Bi_2O_2CO_3$ and BiOCl.

For more directly showing the high photocatalytic activity, the commercial TiO_2 (P25, Degussa Co.) was used as a reference, and the results are shown in Fig. 7. After UV (254 nm) irradiating of 30 min, about 94.5% of RhB was degraded over P25. In stark contrast, the photocatalytic activity of RhB over $Bi_2O_2CO_3$/BiOCl under visible light (420 nm < λ < 800 nm) is even better than that of P25 under UV light (254 nm). Additionally, the total organic carbon (TOC) technique is used to measure the mineralization ratios of organic pollutants over $Bi_2O_2CO_3$/BiOCl and P25, and the results shown in Table S1 indicate that $Bi_2O_2CO_3$/BiOCl possesses the superior capacity of mineralization under visible light or simulated sunlight to P25 under UV light after the same reaction time. Consequently, the $Bi_2O_2CO_3$/BiOCl embodies the photocatalysis superiority in the degradation of RhB.

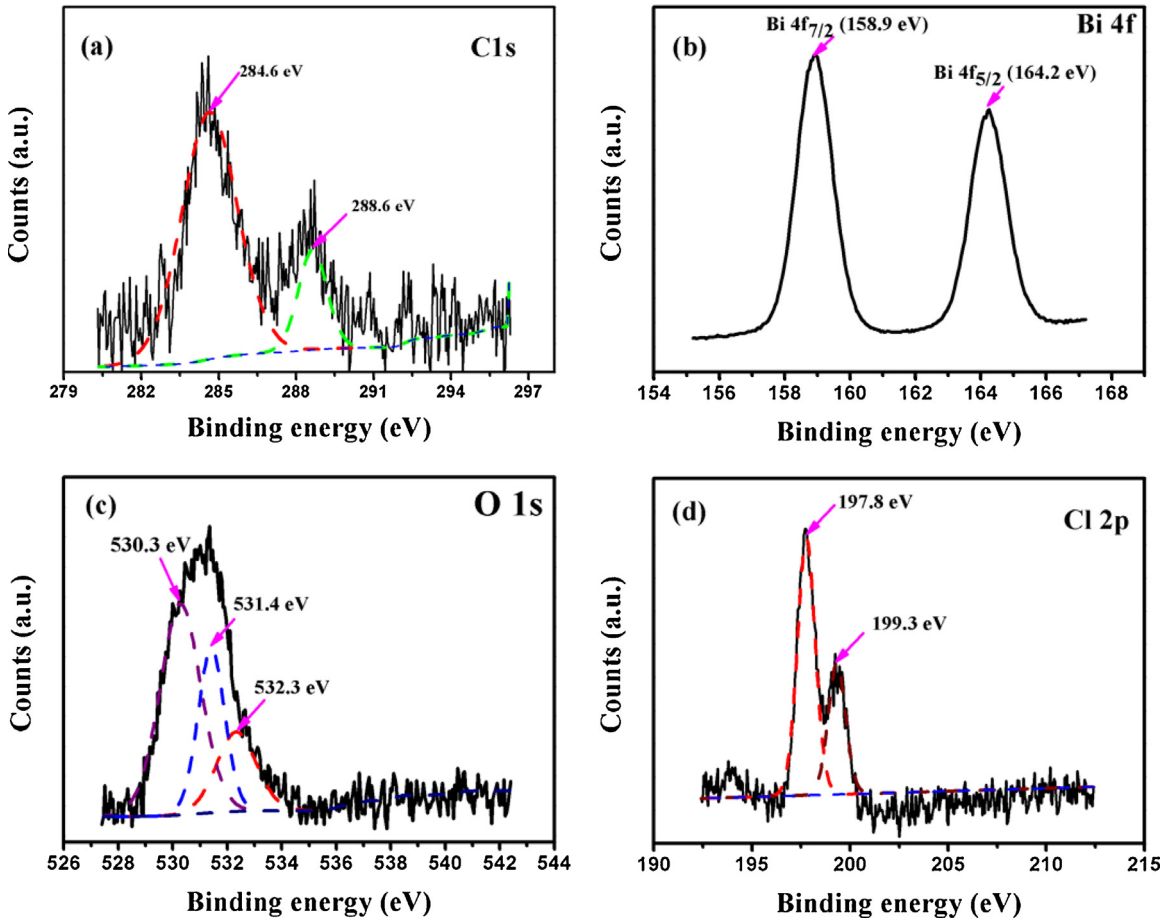

Fig. 4. XPS spectra of the as-prepared heterogeneous $Bi_2O_2CO_3$/BiOCl: (a) C 1s, (b) Bi 4f, (c) O 1s and (d) Cl 2p.

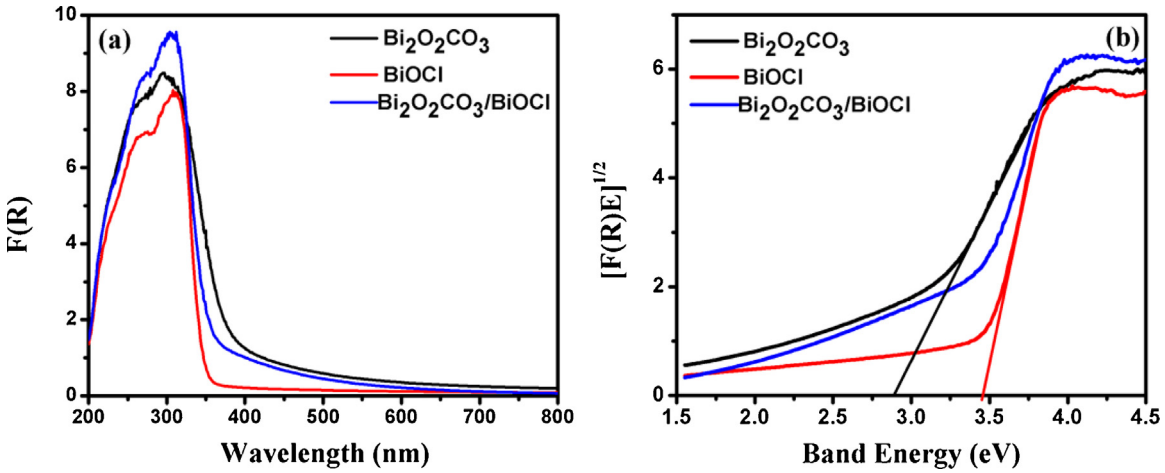

Fig. 5. UV–vis diffuse reflectance spectra (a) and optical bandgap energy Eg (b) of BiOCl, $Bi_2O_2CO_3$/BiOCl and $Bi_2O_2CO_3$.

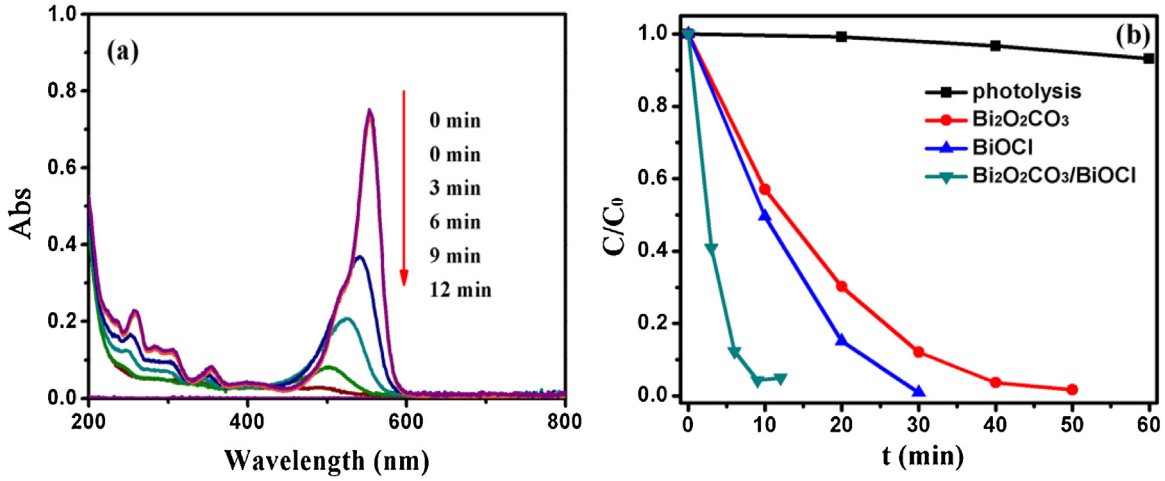

Fig. 6. The absorption spectra (a) of photacatalytic degradation of RhB over $Bi_2O_2CO_3$/BiOCl. Photocatalytic activities (b) of $Bi_2O_2CO_3$, BiOCl and $Bi_2O_2CO_3$/BiOCl under visible light.

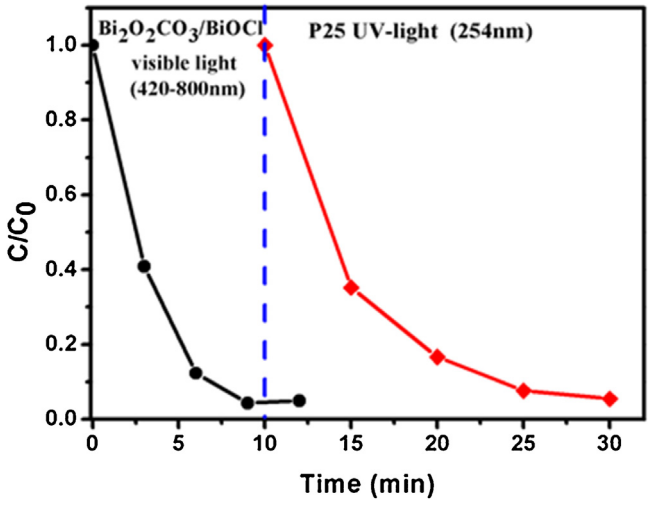

Fig. 7. Photodegradation of RhB over P25 and $Bi_2O_2CO_3$/BiOCl.

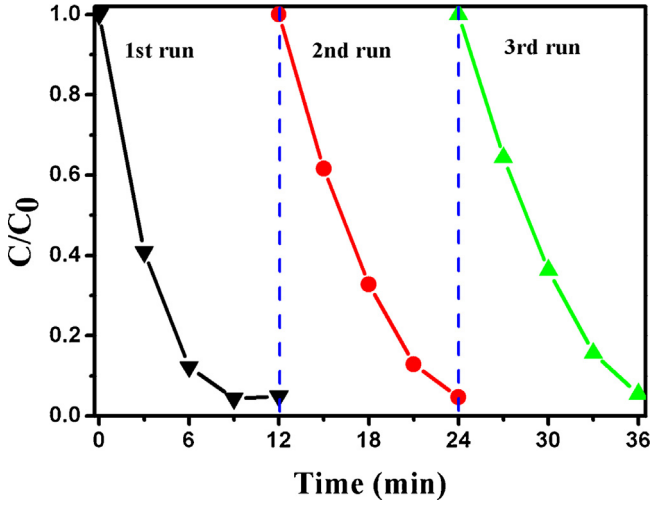

Fig. 8. Photodegradation of RhB over $Bi_2O_2CO_3$/BiOCl photocatalyst during repeated operation under visible light irradiation.

For investigating the stability of the photocatalysts, the recycled experiments for the photodegradation of RhB were carried out, and the results are shown in Fig. 8. When $Bi_2O_2CO_3$/BiOCl catalyst is used for the first time, about 98.0% of RhB could be degraded after 12 min of reaction as shown in the figure. And the degradation rate of the second and third run after 12 min of reaction are 95.4% and 94.5%, respectively. Consequently, $Bi_2O_2CO_3$/BiOCl catalyst is quite stable after three recycles of the photocatalytic degradation

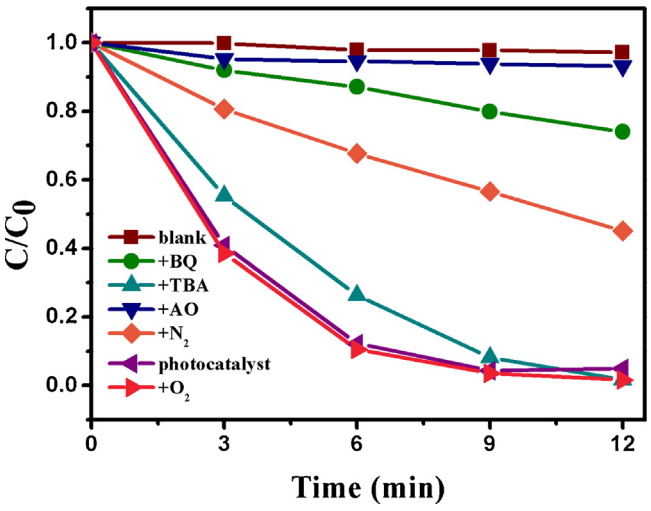

Fig. 9. Photocatalytic degradation of RhB over $Bi_2O_2CO_3$/BiOCl under different conditions with exposure to visible light.

of RhB. Otherwise, the crystallographic phase was hardly changed (Fig. S2(a)), and no changes in surface chemical states were found for the $Bi_2O_2CO_3$/BiOCl after the 3-cycle photocatalytic reaction (Fig. S2(b)), implying that the $Bi_2O_2CO_3$/BiOCl was relatively stable during degradation reaction. Moreover, the recycled experiments under simulated sunlight were also carried out, and the results shown in Fig. S3 predict the potential industry application.

3.3. Photocatalytic mechanism

In order to confirm the involvement of active radical species in the photocatalytic process, the controlled experiments with different types of active species scavengers added in catalyst system are carried out. The photocatalytic activity of $Bi_2O_2CO_3$/BiOCl toward the degradation of RhB under the different conditions is shown in Fig. 9. When 50 mg ammonium oxalate (AO) as a scavenger for holes [38] is added in the system, the degradation rate of RhB is remarkably decreased, from which one can conclude the dominate role of hole in the process of photocatalytic degradation. The benzoquinone (BQ) has the ability to trap $^{\bullet}O_2^-$ by a simple electron transfer mechanism [39] and the addition of BQ (2 mg) provokes partial inhibition of the RhB degradation. In order to further test the role of dissolved O_2 in the degradation process, N_2 was bubbled through the suspension. The rate for degradation of RhB over $Bi_2O_2CO_3$/BiOCl is remarkably decreased in the presence of N_2, which excludes the dissolved O_2 to form $^{\bullet}O_2^-$. It is also demonstrated the important role of $^{\bullet}O_2^-$ in the process of the photocatalytic degradation. With 2 mL of *tert*-butyl alcohol (TBA) as a scavenger for hydroxyl radicals added [40], the rate for degradation of RhB decreases a little, which indicates the less important role of $^{\bullet}OH$ in the reaction. Based the comparison above, it is concluded that the RhB oxidation is driven mainly by the participation of hole and $^{\bullet}O_2^-$ radicals and to a lesser extent by the contribution of $^{\bullet}OH$ radicals.

ESR with 5,5-dimethyl-1-pyrroline-N-oxide (DMPO) technique was carried out to detect the active species under visible light irradiation ($420\,nm < \lambda < 800\,nm$) [41]. There present the signals of the DMPO-$^{\bullet}O_2^-$ with the photocatalysts dispersing in the methanol solution under visible light irradiation, in which peaks for the DMPO-$^{\bullet}O_2^-$ species could be observed with dispersion of $Bi_2O_2CO_3$/BiOCl in methanol as displayed in Fig. 10(a). Herein, the strong signals of DMPO-$^{\bullet}O_2^-$ species reveal the transfer pathway of electrons and demonstrate the important effect of dissolved O_2. Additionally, compared to $Bi_2O_2CO_3$ and BiOCl with faint peaks, $Bi_2O_2CO_3$/BiOCl shows more obvious peak signals under visible light irradiation. While no signals for DMPO-$^{\bullet}OH$ was found in any of the three samples under visible light shown in Fig. 10(b). It is consistent with the controlled experiments of photocatalytic activities (Fig. 9) and further demonstrates the important roles of $^{\bullet}O_2^-$ species and barely contribution of $^{\bullet}OH$ in the photocatalytic degradation reaction.

Mott-Schottky is usually used to measure the flat potential (V_{fb}) of semiconductor particle films [42]. Fig. 11 is the Mott-Schottky plots for P25, $Bi_2O_2CO_3$, and BiOCl film in 0.1 mol/L Na_2SO_4 solution (pH 7). According to Mott-Schottky equation [43], the slopes of the line showed that $Bi_2O_2CO_3$ and BiOCl are all n-type semiconductor and their V_{fb} are −0.52 V and 0.40 V vs. NHE (pH 7) after correction of the Ag/AgCl potencial of 0.22 V (vs. NHE), respectively. It is generally known that the conduction band potential (E_{CB}) of n-type semiconductor is very close to (0.1–0.2 V more negative) V_{fb} [44]. From this, it is deduced that the E_{CB} of $Bi_2O_2CO_3$ is about −0.62 eV, which was more negative than the standard redox potential of $O_2/^{\bullet}O_2^-$ (−0.33 V vs NHE) [43]. While the E_{VB} of $Bi_2O_2CO_3$ is deduced at 2.22 V. The bandgap of the BiOCl was estimated to be 3.42 eV in Fig. 5(b). Hereby, the valance band potential (E_{VB}) of BiOCl is about 3.72 V and is more positive than the standard redox potential of $^{\bullet}OH/OH^-$ (2.38 V vs NHE) [45]. As a result, the photogenerated electrons on irradiated $Bi_2O_2CO_3$ can reduce O_2 to give $^{\bullet}O_2^-$, while the $^{\bullet}OH$ is absent from the system since BiOCl cannot be excited by visible light.

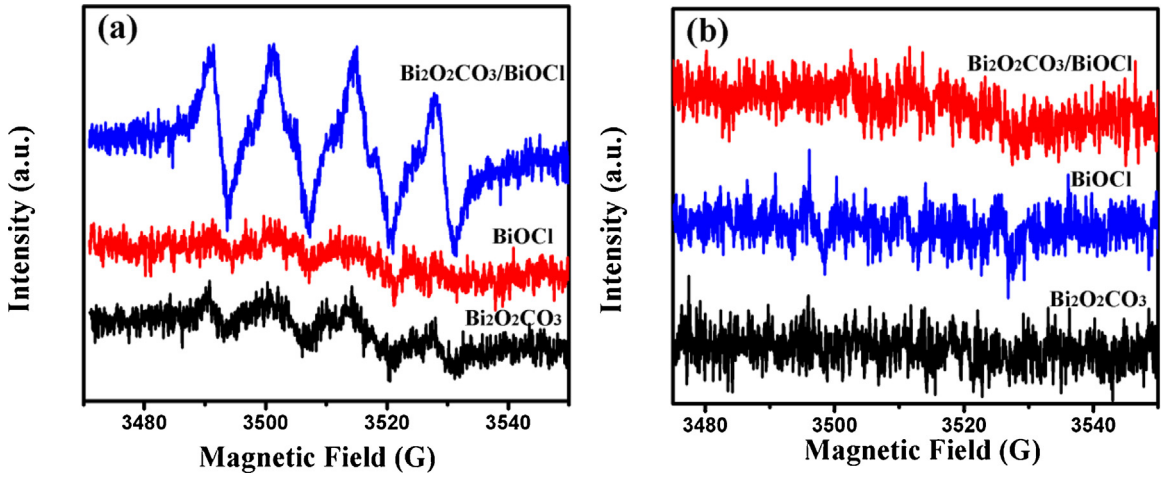

Fig. 10. ESR spectra of DMPO trapped $^{\bullet}O_2^-$ (a) and $^{\bullet}OH$ (b) with the photocatalysts of $Bi_2O_2CO_3$/BiOCl, BiOCl and $Bi_2O_2CO_3$ under visible light irradiation.

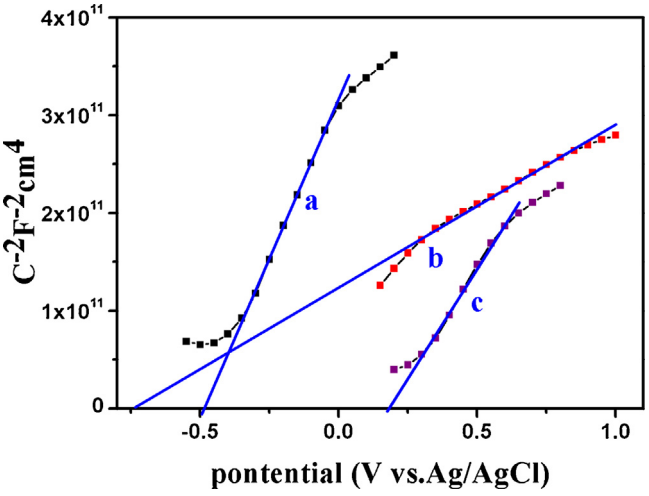

Fig. 11. Mott-Schottky plots of (a) P25, (b) $Bi_2O_2CO_3$ and (c) BiOCl electrodes in 0.1 mol/L Na_2SO_4 at pH 7.

It is well known that RhB has a strongly photosensitization which can facilitate the photocatalytic degradation of itself. In order to determine the degradation of RhB driven by the initial excitation of RhB or the photocatalysts, the combined filters of 500/800 and 420/800 nm (Fig. S4) are applied in the degradation system. Based on the fact that the $Bi_2O_2CO_3$ and BiOCl can only be excited by the wavelength $\lambda < 437$ nm and $\lambda < 363$ nm, and the maximum adsorption peak of RhB locates at 554 nm, the light is filtered by the combined filters of 500/800 nm to exclude the excitation of the photocatalyst while the RhB can be excited.

From the results shown in Fig. 12(a)–(c), the activities decrease to some extend with combined filters of 500/800 nm comparing with that of 420/800 nm for the catalysts of $Bi_2O_2CO_3$ and $Bi_2O_2CO_3$/BiOCl, suggesting the important role of dye photosensitization of RhB and the lesser contribution of the photocatalysts. While it shows barely difference with combined filters of 420/800 and 500/800 nm over BiOCl, inferring the degradation of RhB is completely driven by the excitation of RhB in the degradation system over BiOCl under visible light. By comparing the photocatalytic activities with combined filters of 420/800 nm and 500/800 nm, the conclusion is drawn that the excitation of RhB plays important role in the photocatalytic degradation process, and it is photosensitized reaction over BiOCl.

H_2O_2 is another important intermediate radical species in photocatalysis process and its detection of H_2O_2 can be carried out by the N,N-diethyl-p-phenylenediamine (DPD) method [46]. It is interesting to find the differences in the amount of H_2O_2 in the water and RhB with dispersion of samples under visible light irradiation. The results shown in Fig. 12(d)–(f) indicate that the photosensitization of RhB can increase the production of H_2O_2, and the increments of it are in good accordance with the results in Fig. 12(a)–(c). It is therefore believed that the H_2O_2 predominates in the photosensitization. To further confirm the important role of H_2O_2 in the photosensitization, the experiments of excluding H_2O_2 via adding POD to avoid the existence of H_2O_2 in the reaction system is carried out and the results are presented in Fig. S5. It is found that the activity of BiOCl decreases in the largest extent, and that of $Bi_2O_2CO_3$ and $Bi_2O_2CO_3$/BiOCl decrease in the comparative extent, of which the results are well consistence with that in Fig. 12. From which, we believe that the H_2O_2 increased by the photosensitization affects the photocatalytic activity of BiOCl the most. Therefore, the essence of RhB photosensitization is the increasing of H_2O_2 in the reaction system.

Thus far, we have discussed in detail the optical properties and the excellent photocatalytic property of $Bi_2O_2CO_3$/BiOCl, as well as the roles of the active radical species taking part in the process of the photocatalytic degradation. The excellent photocatalytic activity of $Bi_2O_2CO_3$/BiOCl owes to the heterojunction between $Bi_2O_2CO_3$ and BiOCl. The band alignments result in effective separation and transfer of the photo-induced electrons and holes. On the other hand, the assistance of the dye sensitization further facilitates the degradation of RhB, and the essence of the photosensitization is discussed to be the increasing of H_2O_2 in the reaction system. The

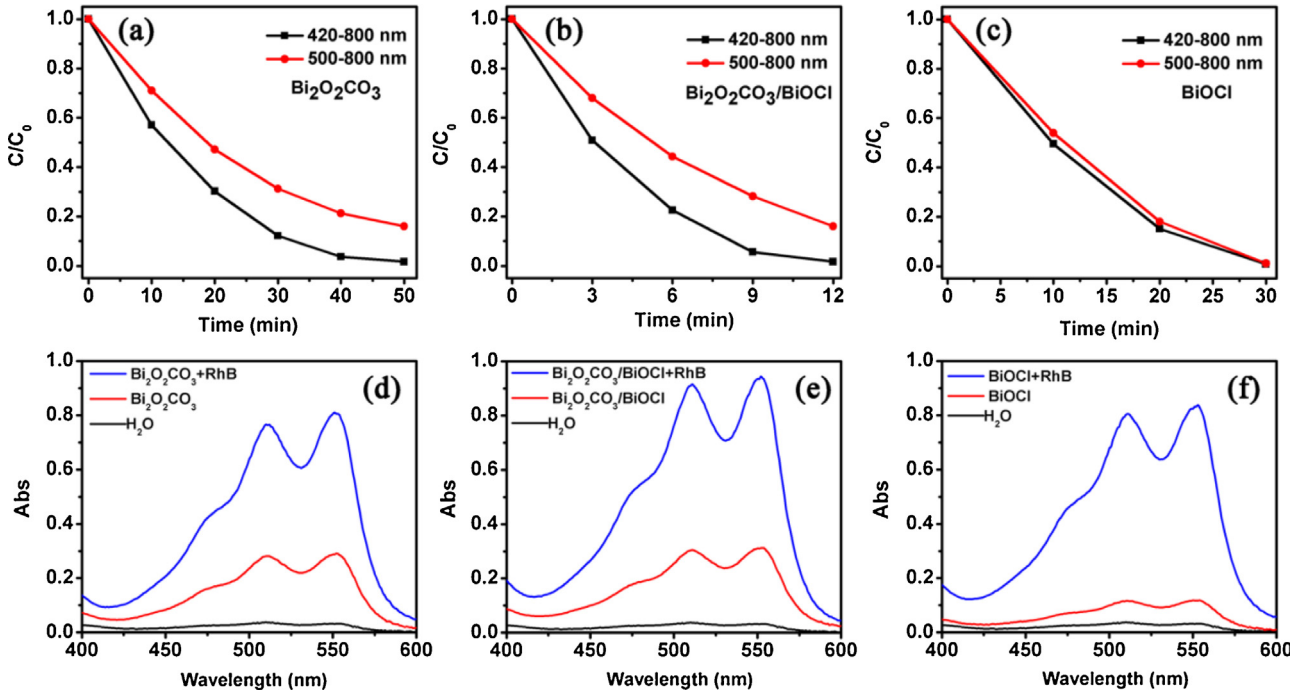

Fig. 12. The photocatalytic degradation of RhB with combined filters of 420/800 and 500/800 nm over $Bi_2O_2CO_3$ (a), $Bi_2O_2CO_3$/BiOCl (b) and BiOCl (c) under visible light. And the detection of H_2O_2 in the water and RhB with dispersion of samples under visible light irradiation (d) $Bi_2O_2CO_3$, (e) $Bi_2O_2CO_3$/BiOCl, (f) BiOCl.

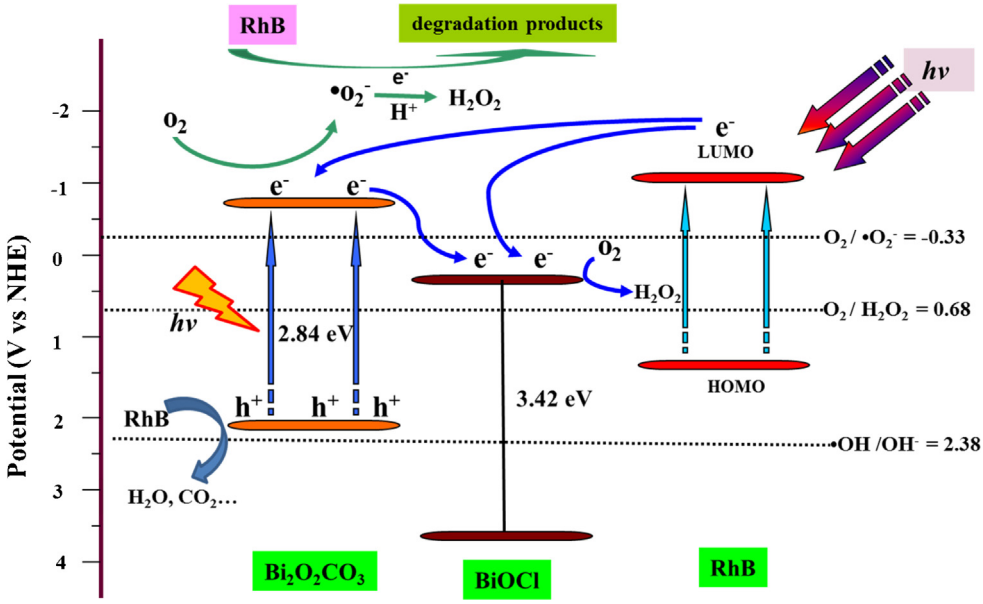

Scheme 1. Proposed mechanism for the visible light photodegradation of RhB over $Bi_2O_2CO_3$/BiOCl heterostructure.

proposed degradation mechanism of RhB over $Bi_2O_2CO_3$/BiOCl and the relationship of band structure between $Bi_2O_2CO_3$ and BiOCl are schematically presented in Scheme 1. A heterojunction is formed after the in-situ growth of BiOCl in $Bi_2O_2CO_3$, which changes the charge transfer process. When $Bi_2O_2CO_3$ is excited by the visible light, the separation of electron and hole occurs. Depend on the negative potential of conduction band of $Bi_2O_2CO_3$ to that of BiOCl, electrons tend to transfer from the conduction band of $Bi_2O_2CO_3$ to that of BiOCl, in which way the separation efficiency of electron-hole pairs in $Bi_2O_2CO_3$ is improved. While the more holes left behind in the valence band would attack the RhB molecule, which is determined to be the very dominate role in the degradation process. Otherwise, as the more negative potential of RhB lowest unoccupied molecular orbital (LUMO) level than the conduction band (CB) of $Bi_2O_2CO_3$ and BiOCl [47,48], the electron transfer from the LUMO of RhB to the CB of $Bi_2O_2CO_3$ is feasible. And the absorption of the visible light over RhB could excites the RhB to form electrons to inject into the conduction band of $Bi_2O_2CO_3$ and BiOCl, which is called dye sensitization producing $^{\bullet}O_2^-$ or H_2O_2 can facilitate the degradation of the RhB molecule. In which way, the alignments of the conduction band and valence band of two materials combined facilitate the production of H_2O_2, which is demonstrated to be the essence of the photosensitization of RhB under visible light. Moreover, the subsequently formed active radical species would as well take part in the oxidation of the RhB. Thus, the heterostructure facilitating photosensitization process over $Bi_2O_2CO_3$/BiOCl toward degradation of RhB is proposed as follows,

$$Bi_2O_2CO_3 + h\nu(\lambda > 420\,nm) \rightarrow Bi_2O_2CO_3(h_{VB}^{+} + e_{CB}^{-}) \quad (2)$$

$$Bi_2O_2CO_3(e_{CB}^{-}) + O_2 \rightarrow {}^{\bullet}O_2^- \quad (3)$$

$$(4)\ {}^{\bullet}O_2^- + 2H^+ + e_{CB}^{-} \rightarrow H_2O_2$$

$$RhB + h_{VB}^{+}({}^{\bullet}O_2^-, H_2O_2) \rightarrow \ldots \rightarrow CO_2 + H_2O \quad (5)$$

$$RhB + h\nu(\lambda > 420\,nm) \rightarrow RhB* \quad (6)$$

$$RhB* + Bi_2O_2CO_3/BiOCl \rightarrow RhB^{+\bullet} + Bi_2O_2CO_3/BiOCl(e^-) \quad (7)$$

$$O_2 + e^- \rightarrow {}^{\bullet}O_2^- \quad (8)$$

$$O_2 + 2H^+ + 2e^- \rightarrow H_2O_2 \quad (9)$$

$$RhB + ({}^{\bullet}O_2^-, H_2O_2) \rightarrow \ldots \rightarrow CO_2 + H_2O \quad (10)$$

4. Conclusions

A facile synthetic approach of the heterostructure of $Bi_2O_2CO_3$/BiOCl was prepared via in-situ growth of BiOCl in precursor of $Bi_2O_2CO_3$. The excellent photocatalytic property of the $Bi_2O_2CO_3$/BiOCl is determined by the photocatalytic degradation of RhB under the visible light. And the photocatalytic activity of the material under visible light is even better than that of P25 under UV light. It is determined that the hole and $^{\bullet}O_2^-$ play very important role in the photocatalytic reaction. Moreover, the facilitation of heterostructure to the photosensitization of RhB for producing more H_2O_2 makes the photocatalytic degradation go more smoothly.

Acknowledgments

This work was financially supported by the NNSF of China (21173047 and 21373049), National Basic Research Program of China (973 Program, 2013CB632405).

Appendix A. Supplementary data

Supplementary data associated with this article can be found, in the online version, at http://dx.doi.org/10.1016/j.apcatb.2016.01.045.

References

[1] Y. Bessekhouad, D. Robert, J.V. Weber, Catal. Today 101 (2005) 315–321.
[2] L. Zhou, W. Wang, H. Xu, S. Sun, M. Shang, Chem.—A Eur. J. 15 (2009) 1776–1782.
[3] Y. Bessekhouad, D. Robert, J.V. Weber, J. Photochem. Photobiol. A: Chem. 163 (2004) 569–580.
[4] D. Robert, Catal. Today 122 (2007) 20–26.
[5] A. Kudo, Y. Miseki, Chem. Soc. Rev. 38 (2009) 253–278.
[6] L. Zhang, D. Chen, X. Jiao, J. Phys. Chem. B 110 (2006) 2668–2673.
[7] C. Zhang, Y.F. Zhu, Chem. Mater. 17 (2005) 3537–3545.

[8] Z.H. Sun, J.J. Guo, S.M. Zhu, L. Mao, J. Ma, D. Zhang, Nanoscale 6 (2014) 2186–2193.
[9] Y. Shimodaira, H. Kato, H. Kobayashi, A. Kudo, J. Phys. Chem. B 110 (2006) 17790–17797.
[10] G.H. Tian, Y.J. Chen, W. Zhou, K. Pan, Y.Z. Dong, C.G. Tian, H.G. Fu, J. Mater. Chem. 21 (2011) 887–892.
[11] C.S. Pan, Y.F. Zhu, Environ. Sci. Technol. 44 (2010) 5570–5574.
[12] C.S. Pan, J. Xu, Y.J. Wang, D. Li, Y.F. Zhu, Adv. Funct. Mater. 22 (2012) 1518–1524.
[13] H. Cheng, B. Huang, K. Yang, Z. Wang, X. Qin, X. Zhang, Y. Dai, Chemphyschem 11 (2010) 2167–2173.
[14] Y. Zheng, F. Duan, M. Chen, Y. Xie, J. Mol. Catal. A: Chem. 317 (2010) 34–40.
[15] L. Chen, R. Huang, M. Xiong, Q. Yuan, J. He, J. Jia, M.-Y. Yao, S.-L. Luo, C.-T. Au, S.-F. Yin, Inorg. Chem. 52 (2013) 11118–11125.
[16] L.Q. Ye, J.Y. Liu, C.Q. Gong, L.H. Tian, T.Y. Peng, L. Zan, ACS Catal. 2 (2012) 1677–1683.
[17] Y. Liu, Z. Wang, B. Huang, K. Yang, X. Zhang, X. Qin, Y. Dai, Appl. Surf. Sci. 257 (2010) 172–175.
[18] L. Chen, S.-F. Yin, S.-L. Luo, R. Huang, Q. Zhang, T. Hong, P.C.T. Au, Ind. Eng. Chem. Res. 51 (2012) 6760–6768.
[19] L. Chen, R. Huang, S.-F. Yin, S.-L. Luo, C.-T. Au, Chem. Eng. J. 193–194 (2012) 123–130.
[20] N. Liang, M. Wang, L. Jin, S. Huang, W. Chen, M. Xu, Q. He, J. Zai, N. Fang, X. Qian, ACS Appl. Mater. Interfaces 6 (2014) 11698–11705.
[21] P. Madhusudan, J. Ran, J. Zhang, J. Yu, G. Liu, Appl. Catal. B: Environ. 110 (2011) 286–295.
[22] G. Cai, L. Xu, B. Wei, J. Che, H. Gao, W. Sun, Mater. Lett. 120 (2014) 1–4.
[23] M. Xiong, L. Chen, Q. Yuan, J. He, S.L. Luo, C.T. Au, S.F. Yin, Dalton Trans. 43 (2014) 8331–8337.
[24] F. Dong, T. Xiong, Y. Sun, H. Huang, Z. Wu, J. Mater. Chem. A 3 (2015) 18466–18474.
[25] T. Xiong, H. Huang, Y. Sun, F. Dong, J. Mater. Chem. A 3 (2015) 6118–6127.
[26] H. Gnayem, Y. Sasson, ACS Catal. 3 (2013) 186–191.
[27] W. Zhang, Q. Zhang, F. Dong, Ind. Eng. Chem. Res. 52 (2013) 6740–6746.
[28] K. Zhang, C. Liu, F. Huang, C. Zheng, W. Wang, Appl. Catal. B: Environ. 68 (2006) 125–129.
[29] X.C. Zhang, T.Y. Guo, X.W. Wang, Y.W. Wang, C.M. Fan, H. Zhang, Appl. Catal. B—Environ. 150 (2014) 486–495.
[30] H. Lu, L. Xu, B. Wei, M. Zhang, H. Gao, W. Sun, Appl. Surf. Sci. 303 (2014) 360–366.
[31] J. Cao, X. Li, H.L. Lin, B.Y. Xu, S.F. Chen, Q.M. Guan, Appl. Surf. Sci. 266 (2013) 294–299.
[32] J. Hu, W. Fan, W. Ye, C. Huang, X. Qiu, Appl. Catal. B: Environ. 158–159 (2014) 182–189.
[33] J. Jiang, K. Zhao, X. Xiao, L. Zhang, J. Am. Chem. Soc. 134 (2012) 4473–4476.
[34] D.H. Wang, G.Q. Gao, Y.W. Zhang, L.S. Zhou, A.W. Xu, W. Chen, Nanoscale 4 (2012) 7780–7785.
[35] H. Wang, Z. Wu, Y. Liu, J. Phys. Chem. C 113 (2009) 13317–13324.
[36] F. Dong, Y. Sun, M. Fu, W.-K. Ho, S.C. Lee, Z. Wu, Langmuir 28 (2011) 766–773.
[37] W. Li, D. Li, Z. Chen, H. Huang, M. Sun, Y. He, X. Fu, J. Phys. Chem. C 112 (2008) 14943–14947.
[38] W. Li, D. Li, W. Zhang, Y. Hu, Y. He, X. Fu, J. Phys. Chem. C 114 (2010) 2154–2159.
[39] R. Palominos, J. Freer, M.A. Mondaca, H.D. Mansilla, J. Photochem. Photobiol. A: Chem. 193 (2008) 139–145.
[40] A.A. Khodja, T. Sehili, J.-F. Pilichowski, P. Boule, J. Photochem. Photobiol. A: Chem. 141 (2001) 231–239.
[41] Z. Wang, W. Ma, C. Chen, H. Ji, J. Zhao, Chem. Eng. J. 170 (2011) 353–362.
[42] G. Redmond, A. O'Keeffe, C. Burgess, C. MacHale, D. Fitzmaurice, J. Phys. Chem. 97 (1993) 11081–11086.
[43] D.A. Aikens, J. Chem. Educ. 60 (1983) A25.
[44] S.R. Morrison, Electrochemistry at Semiconductor and Oxidized Metal Electrodes, Plenum Press, New York, 1980.
[45] Allen J. Bard, Roger Parsons, Joseph Jordan, Standard Potentials in Aqueous Solution, Marcel Dekker Press, New York, 1985.
[46] Y. Lin, D. Li, J. Hu, G. Xiao, J. Wang, W. Li, X. Fu, J. Phys. Chem. C 116 (2012) 5764–5772.
[47] X. Chang, M.A. Gondal, A.A. Al-Saadi, M.A. Ali, H. Shen, Q. Zhou, J. Zhang, M. Du, Y. Liu, G. Ji, J. Colloid Interface Sci. 377 (2012) 291–298.
[48] G. Naresh, T.K. Mandal, ACS Appl. Mater. Interfaces 6 (2014) 21000–21010.